Photoinduced Charge Separation Prompted Intervalence Charge Transfer in a Bis(thienyl)diketopyrrolopyrrole Bridged Donor-TCBD Push-Pull System

Faizal Khan, [a]‡ Youngwoo Jang, [b]‡ Yuvraj Patil, [a] Rajneesh Misra and Francis D'Souza [b]*

Abstract: Intervalence charge transfer (IVCT), a phenomenon observed in molecular systems comprised of two redox centers differing in oxidation states by one unit, is reported in a novel, newly synthesized, multi-modular donor-acceptor system comprised of bis(thienyl)diketopyrrolopyrrole (TDPP) hosting phenothiazine-tetracyanobutadiene (PTZ-TCBD) entities on opposite sides. One-electron reduction of TCBD promoted electron exchange between the two TCBD resulting in IVCT transition in the The stabilization energy, -∆G_{com} and near-infrared region. comproportionation equilibrium constant, Kcom calculated from peak potentials of the split reduction waves were found to be 1.06 x 104 J/mol, and 72.3 M⁻¹, respectively. Further, the IVCT transition was also witnessed during the process of thermodynamically feasible electron transfer upon excitation of the TDPP entity in the system, and served as a diagnostic marker to characterize the electron transfer product. Subsequent transient absorption spectral studies and data analysis by Global and Target analyses revealed occurrence of ultrafast charge separation ($k_{cs} \sim 10^{10} \text{ s}^{-1}$) owing to the close proximity and good communication between the entities of the multi-modular donor-acceptor system. The role of central TDPP in promoting IVCT is borne out from the present investigation.

Introduction

Intervalence (or charge resonance) compounds[1-4]

consisting of two redox centres with different oxidation states connected by a bridge are model systems to study fundamentals of electron transfer events, and also in developing the field of single molecule electronics.[5] Originally, observed in inorganic bis-Ruthenium Creutz-Taube complexes, organic systems are also known to exhibit such phenomenon.[1] Charge localization and delocalization is of importance in mixed valence For one-electron mixed valence compounds comprised of two redox sites connected by a bridge, two extreme cases, viz., Rn+-bridge-R(n+1)+

(complete localization), and $R^{(n+0.5)+}$ -bridge- $R^{(n+0.5)+}$ (full delocalization), and anything in between is possible. Per Robin and Day classification, $I^{[6a]}$ Completely localized systems belong to class I, fully delocalized systems are class III, and systems in between belong to class II. Simple classical theory predicts for class II type to exhibit a highly solvent dependant Gaussian type intervalence charge transfer (IVCT) band in the near-infrared region due to optically induced transfer of the charge from one redox centre to the other. In contrast, for class III type, the IVCT to be asymmetrical (possibly with vibrational fine structure) and largely solvent independent. $I^{[6b,c]}$

3,6-Diaryl-1,4-diketopyrrole[3,4-c]pyrroles (DPPs) are a class of fluorescent compounds known for their strong visible light absorption, photochemical stability, and relatively high carrier mobility. Consequently, they have been widely used in organic electronic applications including singlet fission of producing two triplet excitons in a spin-allowed manner by absorption of a single photon, photovoltaic devices for harvesting light energy and field effect transistors. DPPs can be relatively easily modified at the 2,5-N-lactam or 3,6-aryl group sites for tuning their electronic and photonic properties. Among the functionalized DPPs, 3,6-bis(thiophen-2-yl)diketopyrrolopyrroles (TDPPs), are one of the commonly employed DPP derivatives due to their ease of further functionalization. [8]

NC CN
$$C_{g}H_{17}$$
 NC CN $C_{g}H_{17}$ PTZ-TDPP-TCBD-PTZ, 2

NC CN $C_{g}H_{17}$ PTZ-TDDP, 4

PTZ-TDDP, 4

PTZ-TDDP, 4

PTZ-TDDP, 7

- [a] F. Khan, Dr. Y. Patil, Prof. Dr. R. Misra Department of Chemistry, Indian Institute of Technology, Indore 453552, India. E-mail: raineeshmisra@iiti.ac.in
- [b] Y. Jang, Prof. Dr. F. D'Souza Department of Chemistry, University of North Texas, 1155 Union Circle, #305070, Denton, TX 76203-5017, USA, E-mail: Francis. DSouza@UNT.edu
- ‡ Equal contribution
- Supporting information for this article, experimental and synthetic details, ¹H and ¹³C NMR and HRMS of synthesized compounds. Additional cyclic voltammetric, spectroelectrochemical, computational coordinates, and transient absorption spectral spectra.
- **Figure 1**. Structure of the bis(thienyl)diketopyrrolopyrrole (TDPP) bridged with two phenothiazine-tetracyanobutadiene, (PTZ-TCBD) intervalence charge transfer (IVCT) system investigated in the present study, and the control compounds employed to establish occurrence of IVCT upon one-electron electrochemical reduction, and through the process of photoinduced electron transfer.

Strongly interacting push-pull donor-acceptor systems synthesized by combining electron rich and electron deficient

TDPP-(PTZ)₂, 5

molecular entiteis are known to yield a new type of optical transition in the visible/near-infrared region called intramolecular charge transfer (ICT) that is different from the normal $\pi-\pi^*$ type transitions of individual $\pi\text{-systems}$ (locally excited, LE, transitions) and the above mentioned IVCT transitions. $^{[9]}$ One of the established approaches of synthesizing covalently linked pushpull ICT systems involves linking strong electron acceptors such as tetracyanoethylene (TCNE) or tetracyano-quinodimethane (TCNQ), via a highly facile, catalyst-free [2+2] cycloaddition-retroelectrocyclization reaction involving ethynyl functionalized

electron donor molecules.^[10-13] Few studies, including some from our groups,^[13] have reported on multi-modular push-pull systems by this approach, and have reported on excited state charge transfer events.^[12-14]

In the present study, one of the fundamental questions we would like to address is whether multi-modular systems carrying two or more ICT exhibiting push-pull entities, connected through a central bridge, are able to produce intervalence charge transfer (IVCT) upon reducing one of electron acceptor entities via the process of charge resonance? Although such transition was envisioned earlier,^[15] no experimental proof was provided. The next question we would also like to address is whether such IVCT

band could serve as a diagnostic marker in identifying product of photoinduced electron transfer and help in evaluating kinetics of such event? With this in mind and knowing the ICT exhibiting

properties of Donor-TCBD complexes, and the relative ease of additional functionalization of TDPP via the thienyl entities, we have newly designed and synthesized a multimodular system, 1, shown in Figure 1. This system is comprised of two phenothiazine-tetracyanobutadiene, PTZ-TCBD, ICT exhibiting donorentities symmetrically acceptor connected to the central TDPP (also abbreviated as ((PTZ-TCBD)2-TDPP, 1). Several control compounds were warranted to establish the envisioned goals. Compounds 2 and 3 comprised of only one PTZ-TCBD are the control compounds needed to prove occurrence of IVCT transition in 1 in the near-IR region via electron exchange upon reducing one of its PTZ-TCBD entities. However, owing

to the presence of a single PTZ-TCBD entity in **2** and **3**, these are expected to show an ICT band in the visible region but not IVCT transition in the near-IR region upon reduction. Compounds **4** and **5** are the control compounds lacking TCBD showing no ICT in the ground state or IVCT upon reduction. Finally, compounds **6** and **7** are control PTZ and TDPP needed for their spectral characterizations.

Results and Discussion

Synthesis

The synthesis of ethynyl bridged phenothiazine functionalized TDPPs, **4** and **5** are outlined in Scheme 1. The monobromo TDPP, dibromo TDPP, and ethynyl phenothiazine were synthesized as per reported procedure. The Sonogashira cross-coupling reaction of the monobromo TDPP (**TDPP-1Br**) and dibromo TDPP (**TDPP-2Br**) with 1.1 and 2.2 equivalents of ethynyl phenothiazine resulted in the formation of unsymmetrical **4** and symmetrical **5** in 69% and 73% yields, respectively.

Scheme 1. Synthetic scheme of compounds **PTZ-TDPP**, **4** and **TDPP-(PTZ)**₂, **5**.

Scheme 2. Synthetic scheme of compounds (PTZ-TCBD)₂-TDPP, 1, PTZ-TDPP-(TCBD-PTZ), 2 and PTZ-TCBD-TDPP, 3.

The synthesis of TCBD bridged TDPPs (1, 2 and 3) are outlined in Scheme 2. The reaction of PTZ-TDPP, 4 with tetracyanoethylene (TCNE) in dichloromethane solvent at 40 °C for 8 hours resulted PTZ-TCBD-TDPP, 3 in 91% yield. Compound TDPP-(PTZ)₂, 5 when reacted with controlled equivalents of TCNE in dichloromethane solvent at 40 °C for 8 hours, resulted in the formation of (PTZ-TCBD)₂-TDPP, 1 and PTZ-TDPP-(TCBD-

PTZ), 2 in 87% and 61% yields, respectively. Compound PTZ, 6 was synthesized by the Sonogashira cross-coupling reaction of ethynyl phenothiazine with 2-bromothiophene in the presence of Pd(PPh₃)₂Cl₂ catalyst in 84% yield. The Sonogashira cross-coupling reaction of TDPP-2Br with ethynylbenzene in the presence of Pd(PPh₃)₂Cl₂ catalyst resulted in the formation of TDPP, 7 in 67% yield (Scheme S1). Owing to the presence of two N-C₈ alkyl chains on TDPP, these compounds were found to be readily soluble in common organic solvents such as chloroform, toluene, dichloromethane, and were fully characterized by ¹H and ¹³C NMR and HRMS techniques (see Figures S13–S33 in SI).

Optical absorption and emission studies

Figure 2a illustrates the absorption spectrum of the investigated compounds, normalized to the intense visible peak maxima, in benzonitrile. Compound 6 having no TDPP or TCBD exhibited two peaks at 309 and 358 nm corresponding to the thiophene functionalized PTZ while for compound 7, the main peaks were at 571 and 616 nm due to TDPP absorption. For compounds 4 and 5 having one and two PTZ connected to TDPP, the spectral features were different due to additional contributions from TDPP. For 4 having a single PTZ and a TDPP group, peaks of PTZ at 305 and 359 nm, and at 555 and 590 nm due to TDPP were observed. For 5 having two PTZ entities attached to the central TDPP, all the peaks were red-shifted considerably (~ 40 nm) suggesting some intramolecular type interactions between PTZ and TDPP entities. Finally, for compounds 1 and 2, where one and two ICT exhibiting PTZ-TCBD entities were connected to the central TDPP, red-shifted spectral features were observed. Visible peak maxima at 753 nm for 1, and at 736 nm for 2 was observed. Interestingly, for 3, having only a single PTZ-TCBD arm, the peak maxima was located at 694 nm, however, compared to 4 (its control lacking TCBD), this peak was redshifted by over 100 nm due to ICT contributions of PTZ-TCBD. The results are summarized in Table 1 and nicely demonstrate how the number of π -extending ethyl arms, number of PTZ, and number of PTZ-TCBD attached to on central TDPP govern the optical absorption features of the studied compounds.

Figure 2b shows fluorescence spectra of the investigated series of compounds, excited at their respective visible peak maxima. No fluorescence from TDPP compounds containing highly electron deficient TCBD (compounds 1 to 3) was observed indicating occurrence of excited state events.[17] In contrast, compounds 4 and 5 revealed weaker fluorescence compared to 7 originating from the TDPP entity. Compound 6, having only a PTZ entity revealed PTZ centered emission at 484 nm. Expectedly, the fluorescence lifetimes also showed such a trend (see Figure 2b inset for decay profiles). Lifetimes measured by the time correlated single photon counting (TCSPC) technique nanoLED pulsed excitation sources monoexponential decays for 4-7. Lifetime of 6 was found to be 4.77 ns while that of 5 having two PTZ entities it was 0.16 ns and that of 4 having a single PTZ entity was 0.18 ns. These results indicate quenched singlet emission in 4 and 5 compared to that in 7 (3.17 ns) suggesting excited state events, most likely charge transfer type between relatively electro deficient TDPP and electron rich PTZ entities (vide infra).

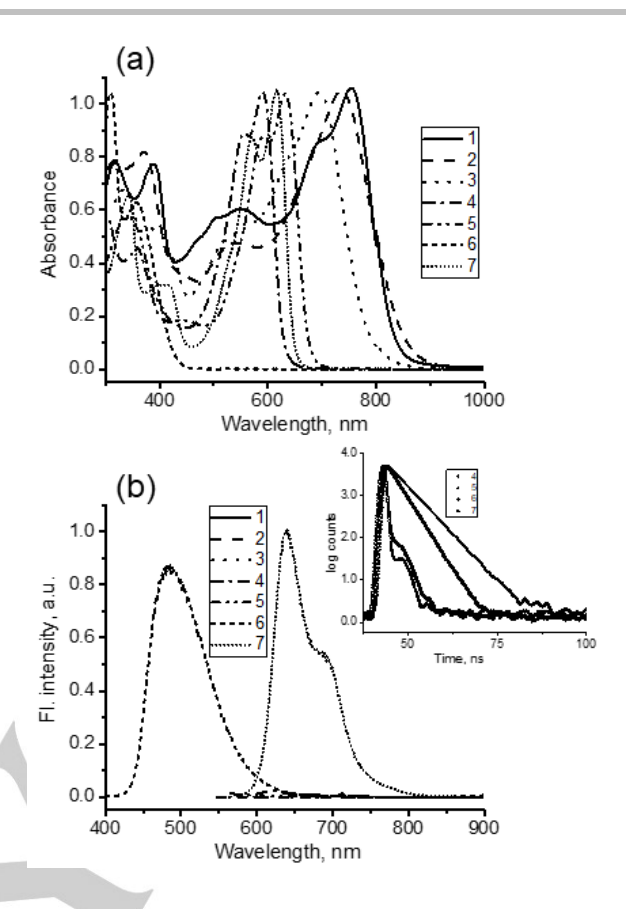


Figure 2. (a) Optical absorption and (b) fluorescence spectra of the indicated compounds in benzonitrile. Samples were excited low energy visible peak maxima. Fluorescence decay profiles of **4**, **5**, **6**, and **7** are shown in Figure 2(b) inset.

Similar absorption spectral trends were observed in nonpolar toluene; however, notable changes were observed in fluorescence. While fluorescence of compounds 1–3 was quantitatively quenched, for compounds 4 and 5 the quenching was considerably low. This was also the trend in the lifetimes, the lifetime of 4 was 2.88 ns while that of 5 it was 2.73 ns compared to that of 7 being 3.17 ns. These results suggest moderate level of excited state interactions in 4 and 5 in nonpolar toluene. Spectra in toluene are shown in Figure S1 and the data are summarized in Table S1.

Electrochemistry and Spectroelectrochemistry

Electrochemical studies coupled electrochemical studies play a pivotal role in visualizing occurrence of intervalence (electron exchange) in multi-modular systems carrying two or more electron donor or electron acceptor entities. In the case of fully delocalized class III type systems or in between class II systems, reduction or oxidation of one of the two redox active entities would split the peaks whose peak separation would depend on the degree of interaction between the two redox active entities. For class I type systems, since the two redox centres are fully localized, the redox processes are expected to occur at the same potential without revealing any splitting. Electrochemical properties were probed using both cyclic (CV) and differential pulse voltammetry (DPV) techniques in DCB containing 0.1 M (TBA)CIO₄ and the potentials were references to Ag/AgCl. The former technique was primarily used to verify the reversibility of the redox processes while the latter was for accurately determine the redox potentials. Figure 3 shows the DPVs of the studied compounds while the CVs are shown in Figure S2 and the potentials are summarized in Table 1.

Table 1. Absorption, emission, redox (in DCB) and free-energy data on the investigated compounds in benzonitrile.

						_	Potential V vs. Ag/AgCl					E	$E_{o,o}$, E_{cT} , ΔG_{sol} , $-\Delta G_{cS}$, $-\Delta G_{cR}$				
Compound $\lambda_{_{abs}}$, nm			$\lambda_{_{\rm Em}}$, nm	τ _{FI} , ns	E reduction			lI	oxidation	eV		eV eV		/ eV			
								TDPP	TCBD	TCBD	PTZ	TDPP					
1	317	390	548	694	753			-1.39	-0.55	-0.02/- 0.13	1.10	1.37	1.56	1.12	-0.49	0.93	0.63
2	317	371	537	736				-0.94	-0.38	-0.14	0.91/ 1.09	1.23	1.57	1.05	-0.49	1.01	0.56
3	336	385	528	694				-1.28	-0.43	-0.18	1.12	1.21	1.74	1.30	-0.49	0.93	0.81
4	305	359	555	590		618 665	0.18	-1.03			0.92	1.11	2.05	1.95			
5	342	448	590	632		662 714	0.16	-0.95			0.91	1.15	1.92	1.86			
6	309	358				484	4.77				0.92		2.94				
7	417	571	616			638 688	3.17	-0.91	/			1.06	1.98				

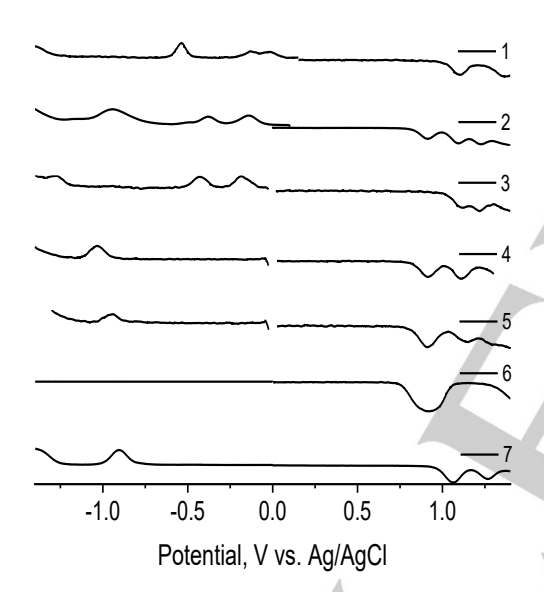


Figure 3. DPVs of indicated compounds in o-dichlorobenzene (DCB) containing 0.1 M (TBA)CIO₄. Scan rate = 5 mVs⁻¹, pulse width = 0.25 s, pulse height = 0.025 V.

Compound 6 with a redox active PTZ entity revealed first oxidation at 0.92 V while TDPP oxidation and reduction in 7 were located at 1.06 and -0.91 V vs. Ag/AgCl. This process was reversible as revealed by corresponding CV curves. Compounds 4 and 5, made out of PTZ and TDPP entities revealed corresponding oxidations and reductions. By comparison with peak currents (one PTZ unit in 4 against two PTZ entities in 5), site of electron transfer for the first oxidation process to the PTZ entity was possible to arrive. For 4, reduction at -1.03 for TDPP and oxidation at 0.92 V for PTZ and at 1.11 V for TDPP while that for 5, reduction at -0.95 V for TDPP and oxidation at 0.91 V for PTZ and at 1.15 V for TDPP entities were observed. Compounds 2 and 3 having all three redox active entities exhibited expected redox peaks. For 3, TDPP reduction at -1.28 V, TCBD reductions at -0.18 V and -0.43 V, and PTZ oxidation at 1.12 V was observed. Similarly for 2, TDPP reduction at -0.94 V, TCBD reductions at -

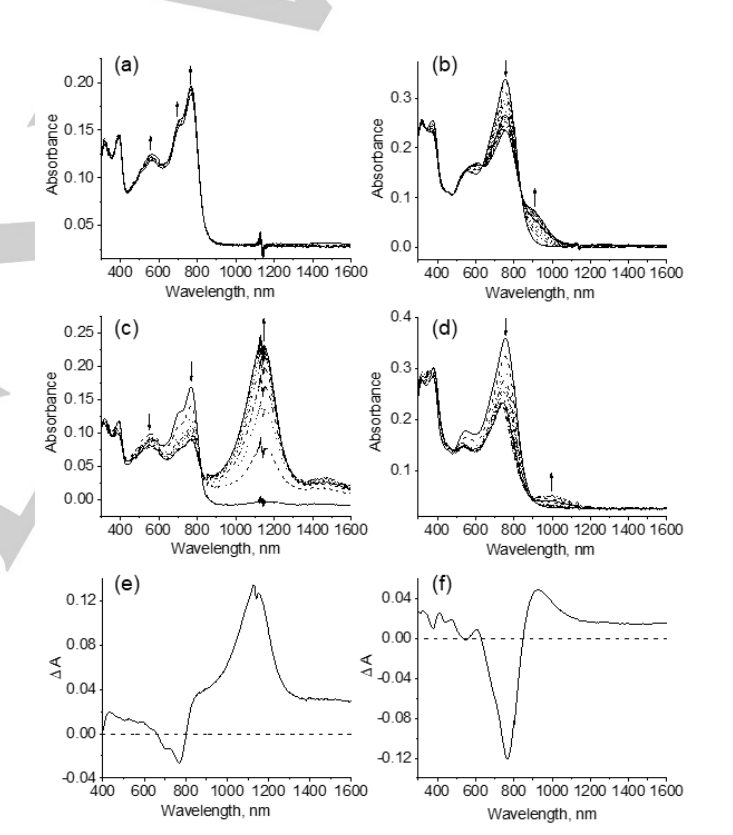


Figure 4. Spectral changes observed during first oxidation and first reduction of compounds $\mathbf{1}$ (a and c) and $\mathbf{2}$ (b and d) in DCB containing 0.2 M TBA(ClO₄). The lower panel shows spectrum deduced for the charge separated state from spectroelectrochemical studies for $\mathbf{1}$ (e) and $\mathbf{2}$ (f).

0.14 V and -0.38 V and PTZ oxidations at 0.91 V (PTZ entity located far from TCBD) and 1.09 V (PTZ entity located close to TCBD) were observed. Finally, compound 1 with two TCBD entities connected with TDPP spacer revealed the expected split for the TCBD first reduction process. In this case, the first reduction was split and appeared at -0.02 V and -0.13 V

(reversible in CV time scale), that is, a 110 mV separation was observed indicating occurrence of electron exchange between the two TCBD entities. Each peak had roughly half the current expected for simultaneous reduction of both TCBD entities. The second reduction involving both TCBD entities appeared at -0.55 V while the TDPP reduction was located at -1.39 V. It may be mentioned here that the central TDPP plays an important role in promoting electronic coupling there by peak splitting. Earlier, no such splitting was observed when truxene (a saturated molecular entity) instead of TDPP was used connecting the TCBD entities. [13b] PTZ oxidation was at 1.10 V close to that observed for compound 3. Overall, presence of TCBD in these multimodular systems made PTZ oxidation harder by about 100 mV and TDPP reduction harder by ~350 mV due to inductive effects caused by the strong electron acceptor TCBD.

The splitting of TCBD waves in 1 upon one-electron reduction is suggestive of electron exchange between the two TCBD entities. As pointed earlier, such phenomenon could result in exhibiting a new IVCT peak in the near-IR region. Advantageously, appearance of such IVCT peak would serve as a diagnostic peak while characterizing products of photoinduced electron transfer upon excitation of TDPP entity (vide infra). With this in mind, spectroelectrochemical studies were systematically performed for both oxidation and reduction processes. Figure 4 shows the spectral changes observed during the process of first oxidation and first reduction of 1 and 2 in DCB containing 0.2 M TBAP while Figure S3 shows such spectral changes for 3 and 5. As shown in Figure 4a, during first oxidation of 1, a small increase in the intensity of the original compound was witnessed without the appearance of any new peaks. This could be attributed to the low molar extinction coefficient values of PTZ.+,[18] compared to intense absorptions of TDPP in the monitoring spectral region. In contrast, during first reduction of 1, decreased original peak intensity was accompanied by intense new peaks at 1136 nm accompanied by a smaller peak at 1471 nm (Figure 4c), characteristic of IVCT via electron exchange between the two TCBD entities. In the case of compounds 2, and 3, having a single TCBD entity, one would not expect such an IVCT transition. This is indeed the case as shown in Figures 4d and Figure S3. In the case of 2, the one-electron oxidized species revealed a less intense peak at 898 nm while the one-electron reduced species revealed weak absorption in the 984 nm region. In the case of 3, no distinctive peak for the oxidized species while a new less intense peak in the 900 nm region for the reduced species was observed. For compounds 5 having only PTZ and TDPP entities, during oxidation weak absorption in the 1000 nm region and no observable new peaks during reduction was observed. summary, the intense near-IR peak was only observed for 1 where IVCT transition was expected. All other compounds, having either one or no TCBD entities such transition was totally absent.

The pair of reduction waves (at -0.02 and -0.13 V) corresponding to one-electron process in the case of $\bf 1$ could be represented as, [1,6c]

Here, the initial production of mixed-valence anion radical is separately followed by its subsequent reduction to the dianionic

species. The difference between the first and second reduction potentials, ΔE = 110 mV reflects the energies of the dianion comproportionation according to equation (ii),

Further, the position of the equilibrium could be quantitatively evaluated from the splitting according to equation (iii),

$$\Delta E = -\Delta G_{\text{com}}/F \tag{iii}$$

where F is the Faraday constant and $-\Delta G_{\text{com}}$ is the Gibbs free-energy change. Then, the main component of the anion-radical stabilization could be estimated according to equation (iv),

$$-\Delta G_{\text{com}} = -RT \ln K_{\text{com}}$$
 (iv)

which represents electronic interaction between the 1/1- redox centers. [6c] The stabilization energy, $-\Delta G_{com}$ and comproportionation equilibrium constant, K_{com} thus calculated from the above approach were found to be 1.06 x 10⁴ J/mol, and 72.3 M⁻¹, respectively.

Computational studies and estimation of electronic coupling parameters

Structures of all the compounds shown in Figure 1 were optimized at the B3LYP/6-31G* basis set and functional using Gaussian 09.[19] Further, frontier orbitals were also generated on the optimized structures using GaussView. In order to expedite the calculations, the N-C₈ chain on the TDPP was replaced by N-C₂ (ethyl) group. Figure 5 shows the optimized structure and frontier orbitals of 1 in the gas phase while for the entire series of compounds is shown in Figure S4 in SI, and the energy of frontier orbitals (HOMO-1, HOMO, LUMO and LUMO+1) are listed in Table S2. In the optimized structures, although closely disposed, no noticeable steric crowding of different entities in the multimodular systems was observed. In the case of 1, the HOMO and HOMO-1 were localized on the terminal PTZ entities while the LUMO and LUMO+1 were delocalized on the central TDPP and TCBD entities (almost symmetric type distribution). In order to check whether the location of the frontier orbitals would differ as a function of solvent polarity, the orbitals were also generated in toluene and acetonitrile, as shown in Figures S5 and S6 (see Table S2 for energies of the orbitals). No significant changes in terms of the location of the frontier orbitals was witnessed.

As shown in Figure S4, for compound **2**, HOMO and HOMO-1 on the TDPP-PTZ entity (PTZ away from TCBD), and LUMO and LUMO+1 on PTZ-TCBD entity was observed. For **3**, HOMO on TDPP extending little on TCBD and LUMO on TCBD-TDPP was observed. For compounds **4** and **5** lacking TCBD, HOMO and HOMO-1 was spread over the PTZ with some contributions on TDPP and LUMO on TDPP was observed. To summarize, the location of frontier HOMO and LUMO mainly tracked that predicted based on the earlier discussed electrochemical site of electron transfer in these multi-modular systems.

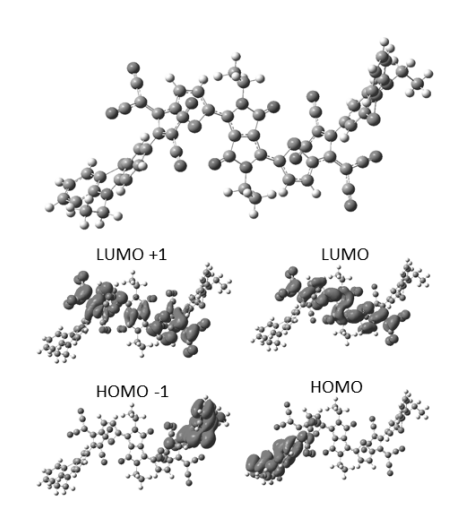


Figure 5. B3LYP/6-31G* optimized structure and frontier orbitals of

Next, an attempt was made to determine the electronic coupling by feeding the optimized structural data to e-Coupling Server program. [20] Details of the calculations are given in the supporting information. By this approach, the estimated electron coupling, H_{AD} = 2V was found to be 2.93 eV that was larger than estimated reorganization energy, λ of 1.56 eV. These results suggest the current IVCT system is a Class III type or a hybrid of Class II and III types. Since IVCT spectrum of Class III type compounds should be largely solvent independent, compound 1 was chemically reduced using cobaltocene as a reducing agent. As shown in Figure S7, the peak position and shape of IVCT transition (main peak in the 1100 nm range with a vibrational band in the 1420 nm range) were almost the same in polar solvents, however, the spectra were blue-shifted in toluene, supporting compound 1 to belong to Class II and III types.

The results presented thus far have unequivocally proven the occurrence of IVCT in **1** upon reduction of one of the TCBD entities. The earlier discussed fluorescence studies revealed TDPP being a fluorescent molecule and that upon connecting the PTZ-TBCD entities undergoes almost quantitative quenching. Due to the strong electron donor and acceptor nature of the entities, excited state electron transfer is a plausible path, and the observation of IVCT peak in the near-IR region upon photoexcitation of **1** would provide experimental evidence for the anticipated charge separation process. With this in mind, free-energy calculations were performed for compounds **1–3** carrying electron acceptor TCBD, the fluorophore TDPP, and donor PTZ. The free-energy for charge separation, $-\Delta G_{CR}$ were estimated according to Rehm-Weller approach^[21] using equations i-iii.

$$-\Delta G_{\rm CR} = E_{\rm ox} - E_{\rm red} + \Delta G_{\rm S} \tag{i}$$

$$-\Delta G_{\rm CS} = \Delta E - (-\Delta G_{\rm CR})$$
 (ii)

where $\Delta E_{0.0}$ corresponds to the excited energy $E_{0.0}$ of ¹TDPP* and E_{CT} is that of PTZ^{δ +}-TCBD $^{\delta$ -</sup> state (calculated from CT peak maxima). The term ΔG_S refers to electrostatic energy calculated according to dielectric continuum model (see equation iii). The E_{ox} and E_{red} represent oxidation and reduction potentials, respectively.

$$\Delta G_S = e^2/4 \pi \varepsilon_0 [-1/R_{cc} \varepsilon_R)$$
 (iii)

The symbols ε_0 and ε_R represent vacuum permittivity and dielectric constant of benzonitrile used for photochemical and electrochemical studies (= 26.0). $R_{\rm CC}$ are the center-to-center distance between donor and acceptor entities from the computed structures. The calculated values are listed in Table 1 which clearly shows thermodynamic feasibility of charge separation.

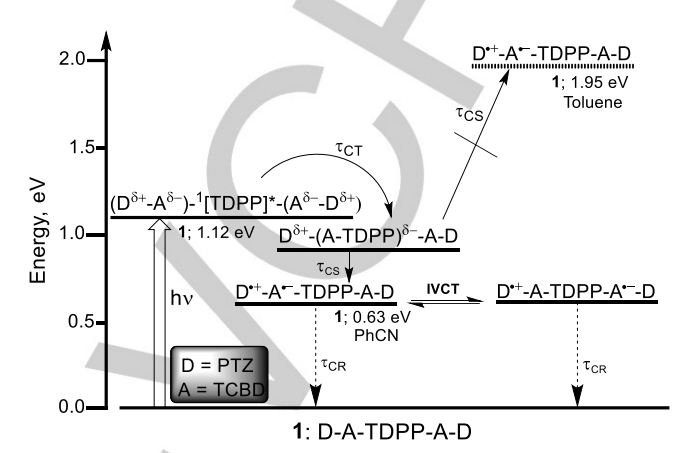


Figure 6. Energy level diagram depicting photoinduced charge transfer and separation processes in 1 in benzonitrile. Energy of charge separated state in toluene is also shown as dashed red line. Abbreviations: CT = charge transfer, CS = charge separation and CR = charge recombination.

Using the calculated energy of different states, energy level diagrams were established to visualize excited state charge transfer and separation processes. Such a diagram for 1 is shown in Figure 6 while for 2 and 3 in Figure S8, and for 4 and 5 in Figure S9, respectively. In the case of 4 and 5 comprised of electron donor, PTZ and a weak electron acceptor TDPP, the singlet excited state energies, $E_{0,0}$ (mid-point energy of absorption and fluorescence peaks) were about 60-100 eV higher than that of the electrochemical HOMO-LUMO gap (difference between the oxidation and reduction potentials, see Table 1) suggesting the possibility of charge transfer type interactions (Figure S9). This is supported by moderate quenching of fluorescence intensities and lifetimes for these two compounds in benzonitrile compared with compound 7 having no PTZ entity(ies) (see Table 1). Incorporation of powerful electron acceptor TCBD in compounds 1-3 would shift the role of TDPP from an electron acceptor to an electron donor. Further, close proximity of TCBD to both TDPP and PTZ entities would promote excited state charge transfer in these push-pull systems, similar to that observed in the ground state in Figure 2. In polar solvent such as benzonitrile, due to solvent stabilization of electron transfer products, the charge transfer state could undergo charge separation, as shown in Figures 6 and S8, however, in nonpolar solvent such as toluene due to poor solvent stabilization such charge separation is energetically not feasible (see dashed red lines in the energy diagrams).

Femtosecond pump-probe studies

In order to understand the excited state features of TDPP, 7 employed in the present study to build the push-pull systems, femtosecond transient absorption studies (fs-TA) covering both

visible and near-IR regions were performed. The sample was excited at the visible peak maxima. As shown in Figure 7, negative peaks at 570 and 630-690 nm, and positive peaks at 778 and 890 nm were observed. By comparison with absorption and fluorescence of TDPP (see Figure 7 for inverse of absorption and emission spectra), the 570 nm peak was attributed to ground state bleach (GSB) and the broad peak in the 630-690 nm for both GSB and stimulated emission (SE). The broad positive peak covering 800-1050 nm with maxima at 890 nm was attributed to excited state absorption (ESA) of ¹TDPP*. Recovery of GSB and SE peaks was tracked decay of the ESA peaks, however, both processes lasted beyond 3 ns, time window of our instrument. This was consistent with the longer lifetime of **7** being 3.17 ns.

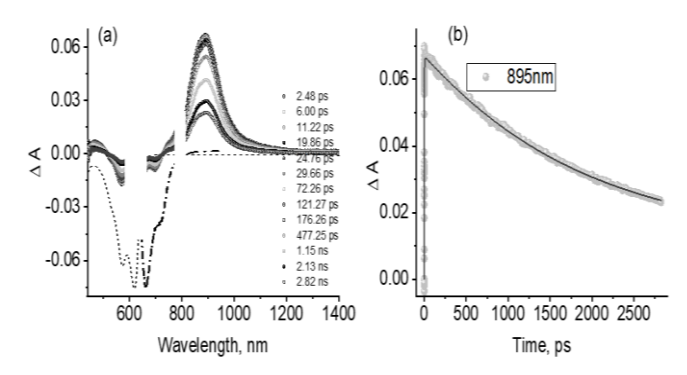


Figure 7. Fs-TA spectra at the indicated delay times of 7 in benzonitrile. The inverse of absorption (purple) and fluorescence (blue) is also included in the spectra. Figure inset shows time profile of the 895 nm peak.

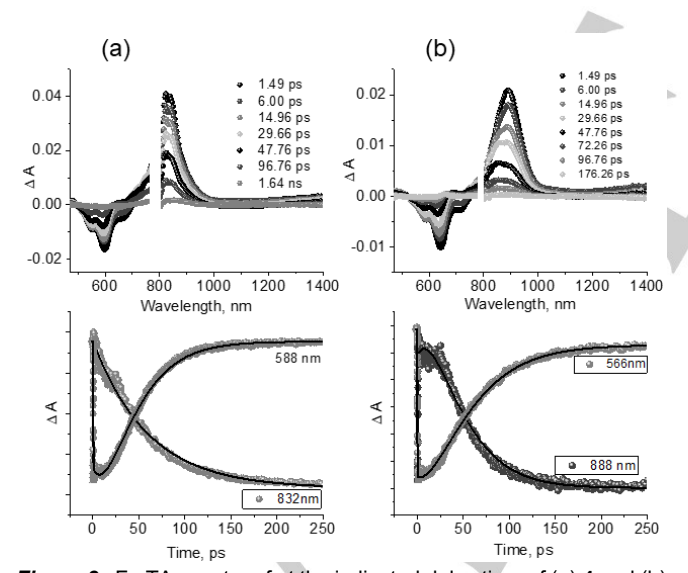


Figure 8. Fs-TA spectra of at the indicated delay time of (a) **4** and (b) **5** in benzonitrile. The samples were excited at visible peak maxima. The rise and decay profiles of the GSB and near-IR peaks at the indicated wavelengths is shown below each panel.

Addition of one or two electron donor PTZ entities on TDPP, compounds **4** and **5**, revealed spectral changes closely resembling that of **7**, as shown in Figure 8 in benzonitrile and Figure S10 in toluene. In these cases, the recovery of GSB and SE peaks, and decay of ESA peak were relatively faster than that observed for **7**, more so for **4** than **5**, a result that is consistent with the earlier discussed fluorescence lifetimes (see time profiles

beneath Figures 8a and b for recovery/decay plots). Importantly, decay of the ESA peak was accompanied by a shoulder peak in both cases (821 nm in the case of **4**, and 854 nm in the case of **5**) and broad absorption in the near-IR region (>1200 nm). Since energy calculations predicted possibility of charge transfer, these peaks have been attributed to the charge transfer species, PTZ^{δ^+} -TDPP $^{\delta^-}$.

Finally, we focussed our attention to compounds **1–3** having TCBD at the centre of PTZ and TDPP entities. As discussed earlier with the help of Figures 2–6, in the case of **1**, one would expect appearance of diagnostic IVCT peak in the near-IR region upon photoexcitation should there be a charge separation from the initial charge transfer state following electron exchange between the two TCBD entities. The spectrum generated for the charge separated state using spectroelectrochemical data, as shown in Figure 4e is highly useful in such analysis.

Figure 9a shows fs-TA spectra at the indicated delay times of 1 in benzonitrile. Spectrum of the charge separated state from spectroelectrochemical studies is also shown for comparison purposes (magenta dashed line). At the earliest delay time, the spectrum revealed negative peaks at 570, 690 and 760 nm corresponding to GSB and a positive peak at 1102 nm. In the 800-900 nm range no new peak was observed that could be attributable to ¹TDPP* suggesting that the excited state is transformed to the charge transfer state within the detection limit of our instrumental setup. With higher delay times the positive peak revealed a red-shift of 24 nm to 1126 nm, close to that separated expected for the state charge from spectroelectrochemical data. Thus, the initial 1102 nm peak could be attributed to the $D^{\delta+}$ -(A-TDPP) $^{\delta-}$ -A-D charge transfer state, while the 1126 nm peak to the charge separated state, D.+-A.-TDPP-A-D undergoing intervalence transfer state, D.+-A-TDPP-A:--D. This becomes obvious when the spectrum was compared with that the spectrum corresponding to the charge separated state from spectroelectrochemical studies (dashed line in Figure 9a). These results support occurrence of photoexcited charge separation resulting in intervalence charge transfer via electron exchange between the two TCBD entities. Further, the transient data was subjected to Glotaran target analysis.[22] A sequential three spectral fitting was needed for better data fitting. The species associated spectra (SAS) for the charge transfer and separation components and their population time profiles are shown in Figure 9b and c, respectively. The first spectrum corresponding to ¹TDPP* appearing within the time resolution of the instrumental setup is not shown for simplicity. The second spectrum with a time constant of 1.31 ps revealed peak maxima at 1086 nm and had features of for the earlier discussed charge transfer state, D^{δ^+} -(A-TDPP) $^{\delta^-}$ -A-D. The final spectrum with a time constant of 4.71 ps revealed peak maxima at 1158 nm for the charge separated intervalence state.

Changing the solvent to nonpolar toluene revealed spectral features distinctly different from those observed in benzonitrile. As shown in Figure S11a, the transient spectra revealed the expected negative peaks and a positive peak at 1078 nm attributable for the charge transfer state. At higher delay times, this peak did not reveal any red-shift, expected for the charge separated state suggesting lack of charge separation in nonpolar toluene, as predicted by the energy level diagram in Figure 6. From Glotaran analysis a time constant for the charge transfer

state of 2.59 ps, slightly higher than that observed in benzonitrile was recorded.

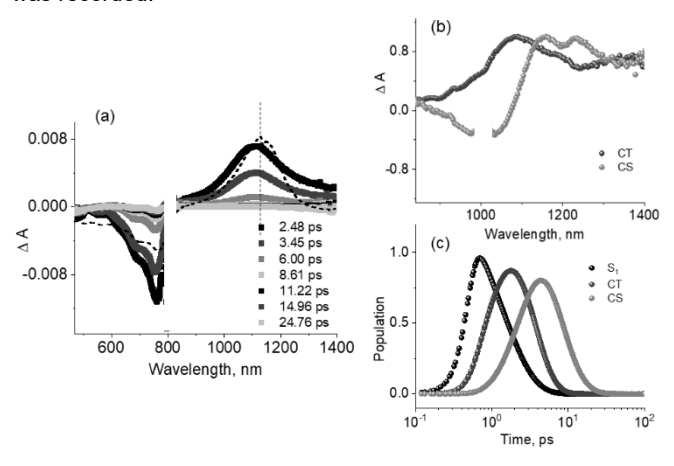


Figure 9. Fs-TA spectra at the indicated delay times of (a) **1** in benzonitrile. Spectrum deduced for the charge separated state from spectroelectrochemical studies is also shown (dashed line) for comparison. The species associated spectra and population kinetics for the data in benzonitrile are shown in b and c, respectively.

In the case of compounds 2 and 3, the earlier discussed spectroelectrochemical studies revealed absence of IVCT type transition as they were comprised of only on TCBD entity. However, free-energy calculations suggested possibility of charge separation in both 2 and 3. With this in mind, both compounds were investigated and the results are shown in Figure 10 for 2 and Figure S12 for 3. The spectrum recorded at a delay time of 3.45 ps revealed GSB peak at 726 nm and a positive peak at 897 nm. Spectra recorded at earlier delay times were mostly structureless possibly due to vibrational relaxation and different degrees of solvation of the singlet excited and charge transfer states. Importantly, the predicted IVCT peak in the near-IR region was missing. The spectrum corresponding to the charge separated from Glotaran analysis agreed well with spectroelectrochemical results suggesting charge separation. Similar results were also observed for 3 in benzonitrile.

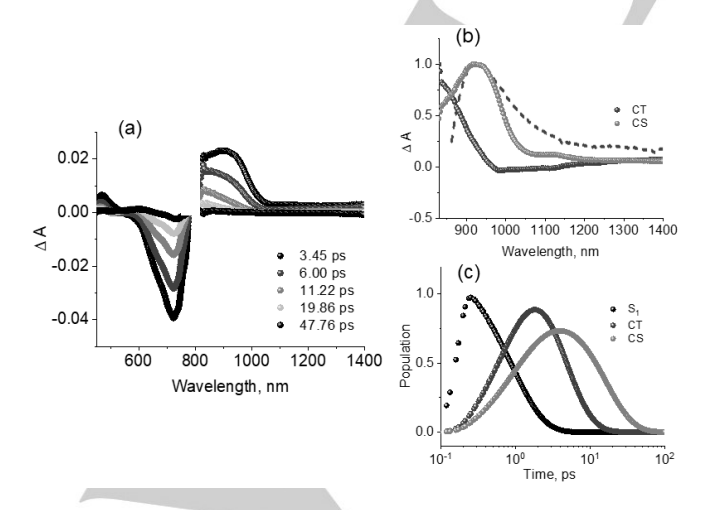


Figure 10. Fs-TA spectra at the indicated delay times of (a) **2** in benzonitrile. (b) The species associated spectra from target analysis along with the spectrum deduced for the charge separated state from

spectroelectrochemical studies. (c) Population kinetics of different states

Fs-TA spectra for compounds **2** and **3** in toluene is shown in Figures S11 b and c, respectively. Formation of charge transfer state from the initial ¹TDPP* was obvious, however, unlike in benzonitrile, no evidence of charge separated state could be secured. Further, Glotaran analysis was performed to evaluate the time constants for different states, as listed in Table 2 below.

Table 2. Time constants for various photo-events from global target analysis of transient data of compounds **1–3** in benzonitrile and toluene.

Compound	λ _{ex} , nm	Solvent	τ _{s1} , ps	τ _{cτ} , ps	τ _{cs} , ps	
PTZ-TCBD-TDPP,	712	PhCN	< 1	1.31	14.12	
		Toluene	< 1	14.25		
PTZ-TDPP-TCBD- PTZ, 2	758	PhCN	< 1	3.65	12.88	
		Toluene	1.35	10.81		
(PTZ-TCBD) ₂ - TDPP, 1	769	PhCN	<1	1.31	4.71	
4		Toluene	< 1	2.59		

From the data presented in Table 2 it is clear that the time constants for the charge transfer states in benzonitrile are short-lived as they transform into the charge separated states. Time constant for the charge separated state in 1 that revealed IVCT transition was relatively shorter compared to those in 2 and 3 having only on TCBD entity. The fs-TA findings demonstrate the significance of electronically communicating TCBD entities in 1 in governing the excited state charge transfer events while providing spectral evidence for the charge separation process in the form of a new intervalence charge transfer band.

Conclusions

In summary, a series of multi-modular push-pull systems comprised of bis(thienyl)diketopyrrolopyrrole, phenothiazine and tetracyanobutadiene were newly synthesized for successful demonstration of intervalence charge transfer in this type of compounds. Appearance of IVCT in 1 was unequivocally demonstrated with the help of several control compounds. Splitting of TCBD reduction wave was the first evidence of electron exchange that was substantiated spectroelectrochemical studies which revealed the anticipated IVCT band in the near-IR region. The stabilization energy, $-\Delta G_{com}$ and comproportionation equilibrium constant, \mathcal{K}_{com} calculated from the electrochemical studies were found to be 1.06 x 104 J/mol, and 72.3 M⁻¹, respectively. The estimated electron coupling, H_{AD} = 2V was found to be 2.93 eV that was larger than estimated reorganization energy, λ of 1.56 eV belonging to Class II and III type. The established energy level diagrams with the help of spectral, electrochemical and computational studies helped in unravelling the photo events in the series of compounds. Charge transfer followed by charge separation in polar benzonitrile but only charge transfer in nonpolar toluene was the main outcome. Detailed photochemistry using femtosecond transient absorption spectroscopy was performed to demonstrate charge transfer and separation events as a function of solvent polarity. Importantly, the near-IR IVCT peak was successfully utilized as a diagnostic marker band to characterize photoinduced electron transfer product in the case of 1. Average lifetime of the charge separated states of compounds 1–3, from Global Target analysis, was in the range of 5–14 ps, demonstrating ultrafast charge separation and recombination processes as a result of the close proximity and good communication between the entities within the multimodular donor-acceptor systems. Further studies along this line are in progress in our laboratories.

Conflict of interest

The authors declare no conflict of interest.

Acknowledgements

This research was supported by the US-National Science Foundation (2000988 to FD), Council of Scientific and Industrial Research (Project No. CSIR 01(2934)/18/EMR-II), New Delhi and SERB (Project No. CRG/2018/000032) New Delhi, Govt. of India. F.K. thanks CSIR-New Delhi (09/1022(0041)/2017-EMR-I) for a fellowship.

Keywords: Intervalence charge transfer, photoinduced charge separation, bis(thienyl)diketopyrrolopyrrole, tetracyanobutadiene, ultrafast spectroscopy.

References and Notes

- a) J. Hankache, O. S. Wenger, Chem. Rev. 2011, 111, 5138-5178; b) A.
 Heckmann, C. Lambert, Angew. Chem. Int. Ed. 2012, 51, 326-392.
- [2] a) I. C. Lewis, I. C. Singer, Chem. Phys, 1965, 43, 2712; b) O. W. Howarth,
 G. K. Fraenkel, J. Am. Chem. Soc. 1966, 88, 4514; c) O. W. Howarth, G.
 K. Fraenkel J. Chem. Phys. 1970, 52, 6258.
- [3] a) J.-P. Launay, Chem. Soc. Rev. 2001, 30, 386; b) N. S. Hush, In Mixed-Valence Compounds; Brown, D. B., Ed.; D. Reidel Publishing Company: Dordrecht, 1980; c) D. E. Richardson, H. Taube, Coord. Chem. Rev. 1984, 60, 107; d) S. F. Nelsen, R. F. Ismagilov, D. A. Trieber, Science 1997, 278, 846.
- [4] a) C. Creutz, H. Taube, J. Am. Chem. Soc. 1969, 91, 3988; b) C. Creutz, H. Taube, J. Am. Chem. Soc. 1973, 95, 1086; c) K. D. Demadis, C. M. Hartshorn, T. Meyer, J. Chem. Rev. 2001, 101, 2655; d) C. Creutz, Prog. Inorg. Chem. 1983, 30, 1; e) W. Kaim, A. Klein, M. Glockle, Acc. Chem. Res. 2000, 33, 755; f) B. S. Brunschwig, C. Creutz, N. Sutin, Chem. Soc. Rev. 2002, 31, 168; g) B. S. Brunschwig, N. Sutin, Coord. Chem. Rev. 1999, 187, 233; h) D. M. D'Alessandro, F. R. Keene, Chem. Soc. Rev. 2006, 35, 424; i) D. M. D'Alessandro, F. R. Keene, Chem. Rev. 2006, 106, 2270; j) J.-P. Launay, Chem. Soc. Rev. 2001, 30, 386. k) M. D. Ward, Chem. Soc. Rev. 1995, 24, 121.
- a) A. Aviram, M. A. Ratner, *Chem. Phys. Lett.*, **1974**, *29*, 277-283; b) H.
 Song, M. A. Reed, T. Lee, *Adv. Mater.*, **2011**, *23*, 1583-1608; c) G. C.
 Solomon, D. Q. Andrews, R. P. Van Duyne, M. A. Ratner, *J. Am. Chem. Soc.*, **2008**, *130*, 7788-7789.
- [6] a) M. B. Robin, P. Day, Adv. *Inorg. Chem. Radiochem.* 1967, 10, 247; b) S. F. Nelsen, *Chem. Eur. J.* 2000, 6, 581; c) N. S. Hush, *Prog. Inorg. Chem.* 1967, 8, 391.
- [7] a) J. Chen, Y. Cao, Acc. Chem. Res. 2009, 42, 1709-1718; b) Y. J. Cheng, S. H. Yang, C. S. Hsu, Chem. Rev. 2009, 109, 5868-5923; c) Y. Lin, L. Ma, Y. Li, Y. Liu, D. Zhu, X. Zhan, Adv. Energy Mater. 2013, 3, 1166-1170; d) Y. Lin, Y. Li, X. Zhan, Adv. Energy Mater. 2013, 3, 724-728; (e) Y. Qiao, Y. Guo, C. Yu, F. Zhang, W. Xu, Y. Liu, D. Zhu, J. Am. Chem. Soc. 2012, 134, 4084-408; f) H. Berckstemmer, A. Weissenstein, D. Bialas, F. Werthner, J. Org. Chem. 2011, 76, 2426-2432; g) J. Dhar, D. P. Karothu, S. Patil, Chem. Commun. 2015, 51, 97-100; h) M. Grzybowski, D. T. Gryko, Adv. Opt. Mater. 2015, 3, 280-320; i) H. Langhals, T. Potrawa, H. Nçth, G. Linti, Angew. Chem. Int. Ed. Engl. 1989, 28, 478-480; Angew. Chem. 1989,

- 101, 497-499; j) M. A. Naik, S. Patil, *J. Polym. Sci. Part A.* **2013**, 51, 4241-4260.
- [8] a) P. E. Hartnett, E. A. Margulies, C. M. Mauck, S. A. Miller, Y. Wu, Y.-L. Wu, T. J. Marks, M. R. Wasielewski, J. Phys. Chem. B 2016, 120, 1357-1366; b) C. M. Mauck, P. E. Hartnett, E. A. Margulies, L. Ma, C. E. Miller, G. C. Schatz, T. J. Marks, M. R. Wasielewski, J. Am. Chem. Soc. 2016, 138, 11749-11761; c) L. J. Huo, J. H. Hou, H. Y. Chen, S. Q. Zhang, Y. Jiang, T. L. Chen, Y. Yang, Macromolecules 2009, 42, 6564-6571; d) B. Walker, A. B. Tomayo, X. D. Dang, P. Zalar, J. H. Seo, A. Garcia, M. Tantiwiwat, T. Q. Nguyen, Adv. Funct. Mater. 2009, 19, 3063-3069; e) Y. Z. Lin, P. Cheng, Y. F. Li, X. W. Zhan, Chem. Commun. 2012, 48, 4773-4775; f) D. Sahu, C. H. Tsai, H. Y. Wei, K. C. Ho, F. C. Chang, C. W. Chu, J. Mater. Chem. 2012, 22, 7945-7953; g) C. Popli, Y. Jang, Y. Patil, R. Misra, F. D'Souza, Chem. Eur. J. 2020, 26, 15109-15115.
- a) M. R. Bryce, Adv. Mater. 1999, 11, 11-23; b) J. W. Verhoeven, J. Photochem. Photobiol C: Photochem. Rev. 2006, 7, 40-60; b) D.L. Sun, S. V. Rosokha, S. V. Lindeman, J. K. Kochi, J. Am. Chem. Soc. 2003, 125, 15950-15963.
- [10] a) T. Michinobu, J. C. May, J. H. Lim, C. Boudon, J. Gisselbrecht, P. Seiler, M. Gross, I. Biaggio, F. Diederich, *Chem. Commun.* 2005, 737-739; b) M. Kivala, C. Boudon, J.-P. Gisselbrecht, P. Seiler, M. Gross, F. Diederich, *Angew. Chem.* 2007, 119, 6473–6477; *Angew. Chem. Int. Ed.* 2007, 46, 6357-6360.
- [11] a) A. Gopinath, N. Manivannan, S. Mandal, N. Mathivanan, A. S. Nasar, J. Mater. Chem. B 2019, 7, 6010-6023; b) T. Michinobu, I. Boudon, J.-P. Gisselbrecht, P. Seiler, B. Frank, N. N. P. Moonen, M. Gross, F. Diederich, Chem. Eur. J. 2006, 12, 1889-1905; c) T. Michinobu, Chem. Soc. Rev. 2011, 40, 2306-2316; d) T. Shoji, S. Ito, K. Toyota, T. Iwamoto, M. Yasunami, N. Morita, Eur. J. Org. Chem. 2009, 4316-4324; e) H. Gotfredsen, T. Neumann, F. E. Strom, A. V. Munoz, M. Jevric, O. Hammerich, K. V. Mikkelsen, M. Freitag, G. Boschloo, M. B. Nielsen, ChemPhotoChem. 2018, 2, 976; f) A. T. Bui, C. Phillippe, M. Beau, N. Richy, M. Cordier, T. Roisnel, L. Lemiegre, O. Mongin, F. Paul, Y. Trolez, Chem. Commun. 2020, 56, 3571-3574; g) M. Yamada, W. B. Schweizer, F. Schoenebeck, F. Diederich, Chem. Commun. 2010, 46, 5334-5336; h) M. Yamada, P. Rivera-Fuentes, W. B. Schweizer, F. Diederich, Angew. Chem. Int. Ed. 2010, 49, 3532-3535.
- [12] a) M. Sekita, B. Ballesteros, F. Diederich, D. M. Guldi, G. Bottari, T. Torres, Angew. Chem. Int. Ed. 2016, 55, 5560; b) K. A. Winterfeld, G. Lavarda, J. Guilleme, M. Sekita, D. M. Guldi, T. Torres, G. Bottari, J. Am. Chem. Soc. 2017, 139, 5520.
- [13] a) P. Gautam, R. Misra, M. B. Thomas, F. D'Souza, Chem. Eur. J. 2017, 23, 9192; b) R. Sharma, M. B. Thomas, R. Misra, F. D'Souza, Angew. Chem. Int. Ed. 2019, 58, 4350; c) Y. Rout, Y. Jang, H. B. Gobeze, R. Misra, F. D'Souza, J. Phys. Chem. C 2019, 123, 23382; d) M. Poddar, Y. Jang, R. Misra, F. D'Souza, Chem. Eur. J. 2020, 26, 6869–6879; e) D. Pinjari, A. Z. Alsaleh, Y. Patil, R. Misra, F. D'Souza, Angew. Chem. Int. Ed. 2020, 59, 23697-23705; f) I. S. Yadav, A. Z. Alsaleh, R. Misra, F. D'Souza, Chem. Sci., 2020, 12, 1109-1120; g) Y. Jang, Y. Rout, R. Misra, F. D'Souza, J. Phys. Chem. B. 2021, 125, 4067-4075.
- [14] a) T. Shoji, S. Ito, K. Toyota, M. Yasunami, N. Morita, Chem. Eur. J. 2008, 14, 8398-8408; b) K. A. Winterfeld, G. Lavarda, J. Guilleme, D. M. Guldi, T. Torres, G. Bottari, Chem. Sci., 2019, 10, 10997.
- [15] A. Khetubol, S. V. Snick, M. L. Clar, E. Fron, E. Coutino-Gonzalez, A. Cloet, K. Kennes, Y. Firdaus, M. Vlasselaer, V. Leen, W. Dehean, M. Van der Auweraer, *Photochem. Photobiol.* 2015, 91, 637-653.
- [16] a) Y. Zou, D. Gendron, R. Badrou-Aı"ch, A. Najari, Y. Tao, M. Leclerc, *Macromolecules* **2009**, 42, 2891-2894; b) Y. Patil, T. Jadhav, B. Dhokale, R. Misra, *Eur. J. Org. Chem.* **2016**, 733-738; c) J. Tan, C. Wang, H. K. Lao, W. Wang, G. Feng, D. Yuan, C. Wu, X. Zhang, *Chem. Commun.*, **2019**, 55, 7438-7441.
- [17] Principles of Fluorescence Spectroscopy, 3rd ed. (Ed.: J. R. Lakowicz), Springer, Singapore, 2006.
- [18] E. Wagner, S. Filipek, M. K. Kalinowski, Monatshefte fur Chemie, 1988, 119, 929-932.
- [19] Gaussian 09, Revision C.01, Gaussian, Inc., Wallingford, CT, USA, 2009.
- [20] a) I. C. de Vaca, A. S. Acebes, G. Victor, J. Comput. Chem. 2016, 37, 1740-1745; b) http://ecouplingserver.bsc.es/
- [21] D. Rehm, A. Weller, Isr. J. Chem. 1970, 8, 259-271.
- 22] a) J. J. Snellenburg, S. P. Laptenok, R. Seger, K. M. Mullen, I. H. M. van Stokkum, J. Stat. Softw. 2012, 49, 1-22; b) http://glotaran.org/

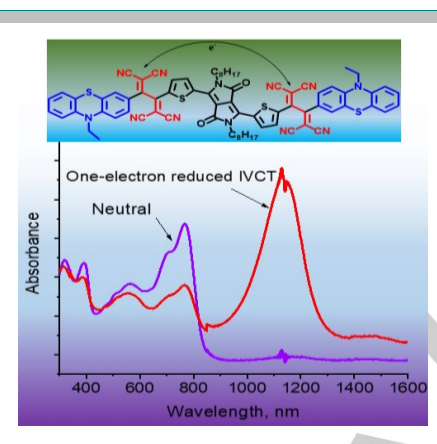
Entry for the Table of Contents

Intervalence Charge Transfer

F. Khan, Y. Jang, Y. Patil, R. Misra* F. D'Souza*

Page No. - Page No.

Photoinduced Charge Separation Prompted Intervalence Charge Transfer in a Bis(thienyl) diketopyrrolopyrrole Bridged Donor-TCBD Push-Pull System



Occurrence of intervalence charge transfer in a newly synthesized multimodular donor-acceptor system comprised of central bis(thienyl) diketopyrrolopyrrole hosting two phenothiazine-tetracyanobutadiene entities on the opposite sides is demonstrated. Further, the near-infrared IVCT band has been used as a diagnostic marker to probe photoinduced electron transfer.

